AIP | The Journal of Chemical Physics

Semiflexible macromolecules in quasi-one-dimensional confinement: Discrete versus continuous bond angles

Aiqun Huang, Hsiao-Ping Hsu, Aniket Bhattacharya, and Kurt Binder

Citation: The Journal of Chemical Physics **143**, 243102 (2015); doi: 10.1063/1.4929600
View online: http://dx.doi.org/10.1063/1.4929600
View Table of Contents: http://scitation.aip.org/content/aip/journal/jcp/143/24?ver=pdfcov
Published by the AIP Publishing

Semiflexible macromolecules in quasi-one-dimensional confinement: Discrete versus continuous bond angles

Aiqun Huang,[1,a)] Hsiao-Ping Hsu,[2,3,b)] Aniket Bhattacharya,[1,c)] and Kurt Binder[2,d)]
[1]*Department of Physics, University of Central Florida, Orlando, Florida 32816-2385, USA*
[2]*Institut für Physik, Johannes Gutenberg-Universität Mainz, Staudinger Weg 9, D-55099 Mainz, Germany*
[3]*Max-Planck-Institut für Polymerforschung, Ackermannweg 10, D-55128 Mainz, Germany*

(Received 26 June 2015; accepted 13 August 2015; published online 28 August 2015)

The conformations of semiflexible polymers in two dimensions confined in a strip of width D are studied by computer simulations, investigating two different models for the mechanism by which chain stiffness is realized. One model (studied by molecular dynamics) is a bead-spring model in the continuum, where stiffness is controlled by a bond angle potential allowing for arbitrary bond angles. The other model (studied by Monte Carlo) is a self-avoiding walk chain on the square lattice, where only discrete bond angles (0° and ±90°) are possible, and the bond angle potential then controls the density of kinks along the chain contour. The first model is a crude description of DNA-like biopolymers, while the second model (roughly) describes synthetic polymers like alkane chains. It is first demonstrated that in the bulk the crossover from rods to self-avoiding walks for both models is very similar, when one studies average chain linear dimensions, transverse fluctuations, etc., despite their differences in local conformations. However, in quasi-one-dimensional confinement two significant differences between both models occur: (i) The persistence length (extracted from the average cosine of the bond angle) gets renormalized for the lattice model when D gets less than the bulk persistence length, while in the continuum model it stays unchanged. (ii) The monomer density near the repulsive walls for semiflexible polymers is compatible with a power law predicted for the Kratky-Porod model in the case of the bead-spring model, while for the lattice case it tends to a nonzero constant across the strip. However, for the density of chain ends, such a constant behavior seems to occur for both models, unlike the power law observed for flexible polymers. In the regime where the bulk persistence length ℓ_p is comparable to D, hairpin conformations are detected, and the chain linear dimensions are discussed in terms of a crossover from the Daoud/De Gennes "string of blobs"-picture to the flexible rod picture when D decreases and/or the chain stiffness increases. Introducing a suitable further coarse-graining of the chain contours of the continuum model, direct estimates for the deflection length and its distribution could be obtained. [http://dx.doi.org/10.1063/1.4929600]

I. INTRODUCTION

Semiflexible polymers confined in narrow channels have found abiding interests recently, both in experiments,[1–14] analytical theory,[15–25] and in computer simulations.[26–39] From the application side, this problem is of great interest for the detection of single DNA molecules, separating them by size, and to develop tools for their sequence analysis. On the theoretical front, confined semiflexible polymers pose a variety of challenging questions: what aspects of the behavior are specific to a particular polymer, and what aspects of the behavior are generic? For fully flexible polymers confined into cylinders with non-attractive walls under good solvent conditions, one expects a fairly universal picture as soon as the cylinder diameter D is much bigger than the size ℓ of an effective segment. Then scaling theory predicts[40,41] that a chain takes a cigar-like conformation of length $L_\parallel \approx Dn_b$ where n_b is the number of "blobs" of diameter D forming a one-dimensional string. Inside each blob self-avoiding walk (SAW) statistics prevails, and hence the number of monomers n per blob satisfies the relation $D \approx \ell n^\nu$, where ν is the Flory exponent,[41] and prefactors of order unity in such scaling arguments are omitted, as usual. Noting that the total number of monomers per chain is $N = n_b n$, one readily concludes $L_\parallel \approx \ell (D/\ell)^{1-1/\nu} N$. This result has been verified by simulations of various coarse-grained models (e.g., Refs. 42–50, 52, and 53).

However, when we deal with semiflexible chains, the persistence length ℓ_p introduces already additional length scales for chains in bulk solution. Indeed, for contour lengths $L = (N-1)\ell$, the chain conformation in a coarse-grained view may resemble a flexible rod of diameter ℓ for $L < \ell_p$, while for $L \geq \ell_p$ in $d = 3$ dimensions, the polymers resemble Gaussian coils, with a mean-square end-to-end distance $\langle R^2 \rangle = 2\ell_p L$, as long as excluded volume effects can be neglected. If one models a semiflexible polymer as a freely jointed chain of rods that have length ℓ_p and diameter w (Fig. 1(a)), one concludes (that in $d = 3$ dimensions) excluded volume effects become relevant[54–57] if L exceeds $L^* \approx \ell_p^3/w^2$ and hence the associated

a)Electronic mail: aiqunhuang@knights.ucf.edu
b)Electronic mail: hsu@mpip-mainz.mpg.de
c)Electronic mail: Aniket.Bhattacharya@ucf.edu
d)Electronic mail: kurt.binder@uni-mainz.de

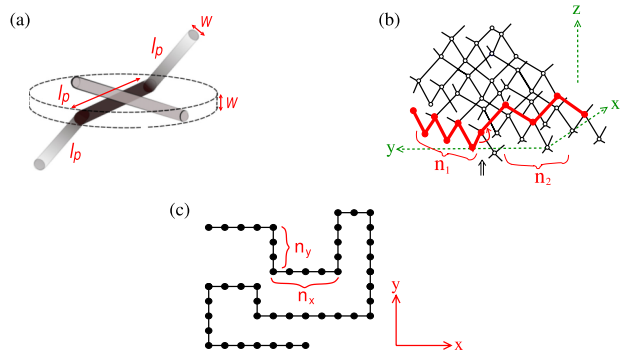

FIG. 1. Some coarse-grained models for semiflexible polymers (schematic). Case (a) shows a model where rigid cylinders of length ℓ_p and diameter w are freely jointed at their links. The excluded volume for a link of another chain (displayed in lighter gray) is a disk of height w and diameter ℓ_p, as indicated by broken lines. This type of model is used as an input for the Flory-theory treatment. Case (b) shows a model for alkane chains with rigid bond lengths and perfect tetrahedral bond angles, so that the chain fits on an ideal diamond lattice (the sites of the lattice are shown by open circles, connected by thin bonds). The monomers (CH_2-groups) are shown as black dots, connected by C–C bonds (thick lines). An all-trans sequence of n_1 bonds (torsion angles $\varphi = 0$ in the all-trans sequence) terminates by a gauche ± state (torsional angle $\varphi = \pm 120°$, highlighted by an arrow) where a differently oriented all-trans sequence of n_2 bonds follows. Case (c) shows a two-dimensional generalized self-avoiding walk model on the square lattice. Due to an energy penalty for ±90° kinks along the chain, the numbers of straight sequences of bonds along the x-axis (n_x) and along the y-axis (n_y) typically are much larger than unity. A possible definition of the persistence length then is $\ell_p = \langle n_x \rangle a = \langle n_y \rangle a$, where a is the lattice spacing.

chain radius $R^* \approx \ell_p^2/w$. For $\ell_p < L < L^*$, the conformation of a semiflexible polymer in $d = 3$ dimensions under good solvent conditions resembles a Gaussian coil, and only for $L > L^*$ does one find swollen coils, $\langle R^2 \rangle \approx \ell_p^{2/5} w^{2/5} L^{6/5}$ (if one uses the Flory estimate[41,58] $\nu = 3/5$ instead of the more accurate estimate[59] $\nu \approx 0.5877$). In $d = 2$, however, this intermediate Gaussian regime is absent,[55,60] and for $L \approx \ell_p$, one immediately crosses over to two-dimensional self-avoiding walk like conformations, with $\langle R^2 \rangle \approx \ell_p^{1/2} L^{3/2}$ (remember $\nu = 3/4$ in $d = 2$).[41,58]

We now draw attention to the length scales of confined semiflexible polymers. For semiflexible chains confined in a cylinder or in a planar slit of diameter (or width) D, the Odijk deflection length[15] (Fig. 2(a))

$$\lambda \approx D^{2/3} \ell_p^{1/3}, \tag{1}$$

which describes the typical length scale over which a chain maintains its orientation in a very narrow channel ($D \ll \ell_p$), gives rise to additional length scales due to hairpin formation,[22,61] such as the typical distance g between neighboring hairpins (Fig. 2(a)), when D is of the same order as ℓ_p. While one expects that semiflexible chains in wide channels ($D \gg \ell_p$) also are compatible with the Daoud-De Gennes[40] picture of a string of blobs, the crossover from the Odijk regime ($D \ll \ell_p$) where $L_\parallel$ differs from L only by a small correction (of order[15,45] $(D/\ell_p)^{2/3}$) to this regime is still a matter of debate.[1,27–31,36] However, we note that Eq. (1) is based on the use of the Kratky-Porod model of wormlike chains[62,63] which describes the polymer in terms of a contour $\vec{r}(s)$ in space, s being a coordinate along this contour, and the Hamiltonian involves a single parameter, the bending rigidity $\kappa_{\rm KP}$,

$$\mathcal{H} = \frac{\kappa_{\rm KP}}{2} \int_0^L ds \left(\frac{d^2\vec{r}}{ds^2}\right)^2. \tag{2}$$

The persistence length ℓ_p is related to $\kappa_{\rm KP}$ via $\ell_p = \kappa_{\rm KP}/k_B T$ (in $d = 3$) or $\ell_p = 2\kappa_{\rm KP}/k_B T$ (in $d = 2$, respectively).

Of course, linear macromolecules are chain molecules where discrete monomers are linked together with covalent chemical bonds along the backbone of a chain; a continuum model such as Eq. (2) can make sense only if the number n_m of such monomers on the length scale ℓ_p is very large. This is the case for double-stranded (ds) DNA, where in typical cases, $\ell_p \approx 50$ nm[64] and $\ell \approx 0.26 - 0.5$ nm;[65] however, when we consider a situation where D is significantly smaller than ℓ_p and two hairpins have to fit into the scale D (Fig. 2(a)), the accuracy of such continuum descriptions seems to us somewhat doubtful. Moreover, it also is of interest to consider also polymers with smaller persistence length, even almost flexible polymers like polyethylene (PE), Fig. 1(b), and polystyrene (PS) exhibit already some local stiffness that needs to be accounted for, and many other rather stiff synthetic polymers exist. Thus, while for PE at $T = 400$ K, $\ell_p \approx 0.75$ nm (and the length ℓ of the C–C bond is 0.15 nm)[66] and for PS corresponding literature estimates[67,68] are $\ell = 0.25$ nm, $\ell_p \approx 1.0 - 1.15$ nm, a comparative study of various synthetic polymers[69] has yielded estimates for ℓ_p in the range from 1 nm to 42 nm, giving also evidence for the double crossover (from rods to Gaussian coils and then to swollen coils) with

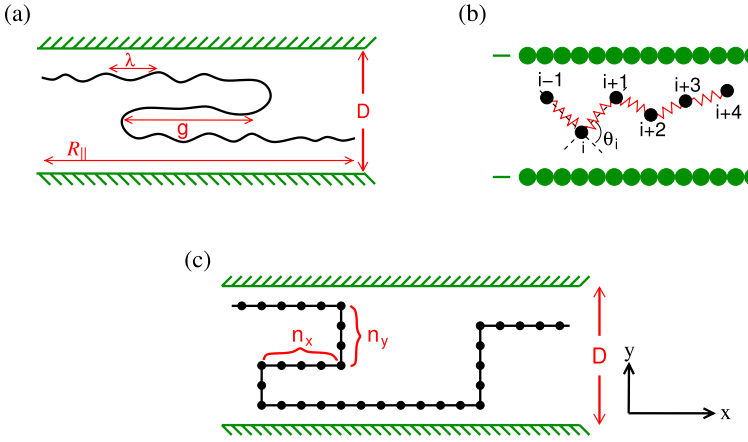

FIG. 2. Some models for confined semiflexible chains: Case (a) shows the Kratky-Porod wormlike chain in a strip of width D, illustrating the definition of the deflection length λ and the typical distance g between neighboring hairpins. Also the component of the end-to-end distance parallel to the boundaries $R_\parallel$ is indicated. Case (b) shows a bead-spring model, where flexibility is controlled by a potential $U_b(\theta_i)$ for the bond angles θ_i. Walls are indicated by particles touching each other. Case (c) shows the model of case (Fig. 1(c)) assuming confinement in a strip of width D, displaying also a lattice analog of a double hairpin configuration.

increasing contour length, in bulk solution under good solvent conditions. For biopolymers one can find examples where $\ell_p \approx 25$ nm (acetan) or $\ell_p = 120$ nm (xanthan),[70] and thus, we prefer not to constrain ℓ_p in our study to a particular value, but rather find it useful to vary it from the fully flexible limit to very stiff chains.

We focus on the fact that for semiflexible polymers, different coarse-grained models are useful (see Fig. 1), depending on the underlying chemistry of the macromolecules that are studied which may differ in their mechanism of flexibility.[71] For dsDNA (under many conditions of interest), there is no conformational disorder on length scales much less than ℓ_p, and flexibility only arises due to the gradual accumulation of the effect of small deviations of valence angles, bond lengths, etc., from their energetically preferred average values. Such deviations inevitably are present due to thermal vibrations.[71] In polymers such as PE and PS, however, the dominating mechanism of flexibility is of the type of the rotational isomeric states (RIS) model,[72] where the chain can be viewed as a succession of all-trans sequences (n C–C bonds where the torsion angle $\varphi = 0$), separated by gauche ($g^{\pm}$) states where the torsional angle is $\pm 120°$ (Fig. 1(b)). The typical length of all-trans sequences is controlled by the depth of the trans-minimum in the torsional potential relative to the gauche minima, and thus strongly temperature-dependent.

In the context of computer simulations, a much simpler model of this type is defined on the square (Fig. 1(c)) or simple cubic lattice, where one models macromolecules simply as self-avoiding walks on these lattices, modeling local chain stiffness via introduction of an energy penalty ϵ_b whenever the walk makes a $\pm 90°$ turn. While this model clearly is only a crude caricature of any real polymer, it shares the property of the alkane-type chains that the local chain contour does not resemble the smooth wormlike chain picture implied by Eq. (2). We feel that different coarse-grained models of semiflexible polymers may be needed for different circumstances: models of the type of Figs. 1(b) and 1(c) may be appropriate for the description of an alkane chain in a carbon nanotube, while the wormlike chain model may be more appropriate for DNA in channels that are 150 nm wide.[1]

Of course, it is well-known particularly for biomolecules that one has to deal there with a multitude of energy scales and length scales, and the optimum choice of a coarse-grained model does depend on the phenomena under study.[73,74] As a disclaimer, we emphasize that the models shown in Figs. 1 and 2 are not meant as an exhaustive list: there are many other interesting models in the literature that we do not discuss here (e.g., Refs. 75 and 76). In our paper we shall also not discuss further the model of Fig. 1(a), although it was used in related studies.[33,38] Here, we shall only focus on a comparison of the two models of Figs. 2(b) and 2(c), both in the bulk and under confinement, to clarify to what extent their properties are universal and to find out what the consequences of different assumptions (such as discrete versus continuous bond angle distributions) are. Also the question to what extent the wormlike chain model (Fig. 2(a)), which ignores the fact that there are individual monomers along a chain rather than a continuous mass distribution, describes the properties of these models accurately will be addressed. Thus, it is the aim of this study to elucidate some general questions on the concept of coarse-graining of macromolecules and study the question which properties of (confined) semiflexible polymers are universal and which are model-dependent.

In Sec. II, the models studied and the simulation methodologies will be briefly summarized. In Sec. III, a comparison of the properties of single chains in bulk (two-dimensional) solution for both models will be given. Sec. IV describes our findings for confined chains, focusing on the case of confinement by repulsive boundaries only. We shall address also the problem of the extent of depletion of monomers near these repulsive walls, since the density profiles of flexible and semiflexible polymers near hard walls are predicted to have characteristic differences.[77] Throughout this work, we pay attention to the fact that the persistence length is a meaningful concept for the local chain stiffness only,[78,79] it must not be associated with the decay of long range orientation correlations along the chain contour. Sec. V finally summarizes our conclusion.

II. MODELS AND SIMULATION METHODOLOGY

In this paper, we consider models in $d = 2$ space dimensions only. Although this restriction precludes a direct comparison of our results with most experimental work, there is the major simplifying feature, that unconfined semiflexible polymers exhibit a single crossover, from rods to self-avoiding walk like chains.[55–57,80] The intermediate region of Gaussian random walk-like chains does not occur, and there is evidence to believe that this intermediate regime complicates the crossover behavior of confined semiflexible polymers considerably (see, e.g., Refs. 29 and 30). Also the complication that knots may form (which is relevant for dsDNA in various circumstances[81,82]) cannot occur in $d = 2$. Our preliminary work[34,36] on confinement effects on chains in $d = 2$ already has indicated a rather complex behavior, and hence in the present work, we shall address this problem in more detail, with an emphasis on the question to what extent the phenomena are universal and which aspects are model-dependent. Hence, we shall contrast results for the lattice model of Figs. 1(c) and 2(c) with results for the bead-spring model of Fig. 2(b) and shall explore to what extent the predictions of the Kratky-Porod wormlike chain model in the continuum (Fig. 2(a)) can be verified.

In our lattice model, each effective monomer occupies a lattice site of the square lattice, and the bond length ℓ between nearest neighbors along the chain is just the lattice spacing, taken as a unit of length for this lattice, so the contour length L, related to the number of beads N as $L = (N-1)\ell$ also is an integer. Both for this model and the continuum bead-spring model we assume that the standard bond bending potential (θ is the angle between subsequent bonds along the chain)

$$U_b(\theta) = \epsilon_b(1 - \cos\theta). \tag{3}$$

On the lattice, however, only angles $\theta = 0°$ and $\pm 90°$ are permitted ($\theta = 180°$, i.e., immediate reversals are forbidden by excluded volume, of course) and so $U_b(\theta) = 0$ if the SAW continues straight on, while $U_b(\theta) = \epsilon_b$ if it makes a kink. The partition sum of the semiflexible SAW hence can be written as

a polynomial in the Boltzmann factor $q_b = \exp(-\epsilon_b/k_BT)$,

$$Z_N(q_b, D) = \sum_{\text{config.}} C_{N,N_{\text{bend}}}(D) q_b^{N_{\text{bend}}}. \quad (4)$$

Here, the sum over configurations includes all SAW's with y coordinates of the monomers in the range $1 \le y \le D$, to realize the confinement by repulsive (one-dimensional walls) placed at $y = 0$ and $y = D + 1$ (so the geometric distance between the walls is $D + 1$). Of course, the limit $D \to \infty$ means we consider an unconfined polymer.

This problem can be studied very efficiently with Monte Carlo (MC) simulations applying the pruned-enriched Rosenbluth method (PERM).[57,83,84] This chain growth algorithm with "population control" and "depth-first implementation" has been thoroughly reviewed in Ref. 84, where the reader can find more details. We could study chain lengths up to $N \sim 10^5$, for a wide variety of chain stiffness, varying $q_b = 1.0$ (fully flexible chains) to $q_b = 0.005$ (rather stiff chains, with a persistence length[34,57] $\ell_p \approx 118\ell$). Note that both for the lattice model and the continuum model the persistence length is extracted from $\langle \cos\theta \rangle$ via

$$\ell/\ell_p \equiv -\ln(\langle \cos\theta \rangle). \quad (5)$$

We recall that the persistence length has a physical meaning (for real polymer chains) only as a characteristic for the local angular correlation between neighboring bonds but cannot be interpreted in terms of orientational correlations for large chemical distances along the chain:[57,78,79] the textbook formula[58] $\langle \cos\theta(s) \rangle \propto \exp(-\ell s/\ell_p)$ for the angular correlation of bonds a chemical distance ℓs apart along the contour holds only for Gaussian phantom chains, while in reality $\langle \cos\theta(s) \rangle$ decays with a power law in s. We emphasize this simple point again, because the misleading textbook formula still is widely used in the literature, without being aware of its limitations (it makes sense only for $\ell s < \ell_p$, of course). The persistence length as defined in Eq. (5), however, can be related to the stiffness parameter κ_{KP} of the Kratky-Porod model, since for stiff chains $\langle \cos\theta \rangle$ is close to unity and hence $\ell/\ell_p \approx \langle \theta^2 \rangle/2$.

If excluded volume could be neglected on the local scale, we would have $\langle \cos\theta \rangle = 1/(1 + 2q_b)$ in $d = 2$ and hence $\ell_p/\ell \approx 1/(2q_b)$ for small q_b. The data (Table I[57]) rather imply $\ell_p/\ell \approx 0.61/q_b = 0.61 \exp(\epsilon_b/k_BT)$. This exponential dependence between ℓ_p and ϵ_b is a characteristic of the lattice model (since thermal activation is required to make a bend), but a similar variation can also be expected for the alkane-type chains (Fig. 1(b)), where the energy difference between the gauche ± and trans-minima of the torsional potential would correspond to ϵ_b.

TABLE I. Estimates of the persistence length ℓ_p/ℓ (Eq. (5)) of polymer chains in the bulk for the lattice model and the continuum model.

Lattice			Continuum			
q_b	ϵ_b	ℓ_p/ℓ	κ	ℓ_p/ℓ	κ	ℓ_p/ℓ
1.0	0	1.06	1.5	2.74	48.0	79.04
0.4	0.92	2.00	2.0	3.30	64.0	105.60
0.2	1.61	3.50	3.0	4.58	96.0	159.10
0.1	2.30	6.46	4.0	6.05	128.0	212.40
0.05	3.00	12.35	6.0	9.25	192.0	319.10
0.03	3.51	20.21	8.0	12.56	320.0	532.50
0.02	3.91	30.02	12.0	19.27		
0.01	4.61	59.22	16.0	25.91		
0.005	5.30	118.22	32.0	52.62		

The bead-spring model used by us describes excluded volume interactions between the monomers by the standard short range Lennard-Jones (LJ) potential $U_{\text{LJ}}(r)$ that is cut off in its minimum and shifted to zero, r being the distance between monomers,

$$U_{\text{LJ}}(r) = 4\epsilon[(\frac{\sigma}{r})^{12} - (\frac{\sigma}{r})^{6}] + \epsilon, \text{ for } r \le 2^{1/6}\sigma, \quad (6)$$

$$U_{\text{LJ}}(r) = 0 \text{ for } r > 2^{1/6}\sigma. \quad (7)$$

Here, σ is the effective diameter of a monomer and ϵ the strength of the potential. The connectivity between neighboring monomers along the chain is ensured by using the Finitely Extensible Nonlinear Elastic (FENE) potential[85]

$$U_{\text{FENE}}(r) = -\frac{1}{2} k R_0^2 \ln(1 - r^2/R_0^2), \quad (8)$$

where $R_0 = 1.5\sigma$ is the maximum extension of the spring, and k the spring constant. We choose σ as the unit of length for this off-lattice model and ϵ/k_B as the unit of temperature T. Choosing $T = 1.2$ throughout and $k = 30$, the average bond length $\ell = 0.971$ and we find that this length does not depend on the choice of the parameter ϵ_b in Eq. (3), which we use here as a bond bending potential as well. However, unlike the case of the lattice model, a continuous range of bond angles θ from $\theta = 0$ to (almost) $\theta = \pi$ is possible, and the parameter ϵ_b now can be related to the rigidity parameter κ_{KP} of the Kratky-Porod wormlike chain model, as is well-known (see, e.g., Ref. 80 where it is shown that $\kappa_{KP}/\ell = \epsilon_b$). In order to easily distinguish in the present paper the data of the continuum model from those of the lattice model, we shall define $\kappa \equiv \epsilon_b$ for the data of the continuum model, to remind the reader that this parameter (apart from the factor ℓ which is very close to unity anyway) essentially measures the chain rigidity in the usual way. Likewise, the "chain length N" for long chains in our units is numerically very close to the contour length L (strictly speaking, $L = (N - 1)\ell$, of course). The potential for the monomer-wall interaction is chosen in full analogy to Eqs. (6) and (7), namely, when we orient the walls along the x-axis, we have

$$U_{\text{wall}}(y') = 4\epsilon[(\frac{\sigma}{y'})^{12} - (\frac{\sigma}{y'})^{6}] + \epsilon \text{ for } y' \le 2^{1/6}\sigma, \quad (9)$$

$$U_{\text{wall}}(y') = 0 \text{ for } y' > 2^{1/6}\sigma, \quad (10)$$

and $y' = y$ at the lower wall while $y' = D - y$ at the upper wall.

When we compare the continuum model to the lattice model, the correspondence of what a particular strip thickness means is somewhat subtle. On the lattice, the geometric distance between the two walls is $D + 1$ lattice spacings, but only a region of extent D (lattice rows $n = 1, 2, \ldots, D$) is accessible for occupation by the monomers of the chain. In the continuum, the full range $0 < y < D$ is in principle accessible for the monomers, but due to the repulsive potential, the regions $0 < y < \sigma/2$ and $D - \sigma/2 < y < D$ are practically almost

excluded for the monomers. Thus, one could argue that the parameter D of the continuum model should be compared to the parameter $D + 1$ of the lattice model. Such ambiguities in the comparison will not matter if D is very large, of course. To be better able to compare data of both models directly, we shall introduce the notation of an effective strip thickness D_{eff}, with $D_{\text{eff}} = D + 1$ in the lattice case and $D_{\text{eff}} = D$ for the continuum model.

For the off-lattice model, chain configurations are equilibrated by using standard Molecular Dynamics (MD) methods applying the Langevin thermostat as usual,[85] for all monomers $i = 1, \ldots, N$,

$$md^2\vec{r}_i/dt^2 = -\nabla(U_{\text{LJ}} + U_{\text{FENE}} + U_b + U_{\text{wall}}) - \Gamma d\vec{r}_i/dt + \vec{f}_i^R(t), \tag{11}$$

where m is the mass of a monomer (we choose units such that $m \equiv 1$), $\vec{r}_i(t) = (x_i(t), y_i(t))$ is the position of monomer i at time t, Γ is the monomer friction coefficient, and $\vec{f}_i^R(t)$ is a random force, satisfying the standard fluctuation dissipation relation (remember we deal with $d = 2$ dimensions)

$$\langle \vec{f}_i^R(t) \cdot \vec{f}_j^R(t') \rangle = 4k_B T\Gamma\delta_{ij}\delta(t - t'). \tag{12}$$

The reduced unit of time then is $(m\sigma^2/\epsilon)^{1/2}$, and this set of equations of motion then is integrated with the reduced time step $\Delta t = 0.01$, applying the algorithm of van Gunsteren and Berendsen.[86] Typically the length of the runs was 1000×10^6 time steps.

We note that slightly more complicated models of this type can serve as coarse-grained models for chemically specific macromolecules exhibiting some angular rigidity, e.g., polyvinyl alcohol,[87] but this is not our focus here.

III. SINGLE CHAINS IN BULK DILUTE SOLUTION: A COMPARISON BETWEEN THE LATTICE AND THE CONTINUUM MODEL

In this section, we demonstrate that the scaled mean square end-to-end distance and the scaled mean square transverse fluctuation of two-dimensional semiflexible chains of contour length L exhibit an almost universal behavior, when one studies these quantities as a function of the dimensionless parameter L/ℓ_p, i.e., measuring the contour length in units of the persistence length.

Of course, such a type of scaling is already suggested by the Kratky-Porod model,[62,63] which would yield for the mean-square end-to-end distance $\langle R_N^2 \rangle$ for a wormlike chain,

$$\langle R_N^2 \rangle/(2\ell_p L) = 1 - \frac{\ell_p}{L}[1 - \exp(-L/\ell_p)]. \tag{13}$$

Evidently for $L \ll \ell_p$ the chain behaves like a rigid rod, $\langle R_N^2 \rangle = L^2$, while the limiting behavior for $L \gg \ell_p$ is that of a Gaussian coil, $\langle R_N^2 \rangle = 2\ell_p L$. Thus, it is natural to provide a plot of our simulation results in the normalization suggested by Eq. (13), studying $\langle R_N^2 \rangle/(2\ell_p L)$ as a function of L/ℓ_p (Fig. 3(a)). It is seen that on the log-log plot there are essentially two regimes of straight lines, with slopes of unity and one half, respectively. The regime with slope unity is the rod-like regime expected from Eq. (13), and there the lattice and continuum results precisely superimpose, which is no surprise at all, of course. As expected, the rod regime stops near $L/\ell_p \approx 1$. While Eq. (13) would predict for $L/\ell_p \gg 1$ a horizontal plateau, i.e., slope = zero on the log-log plot, this regime of Gaussian behavior is completely absent. This breakdown of the Kratky-Porod model in $d = 2$ dimensions due to excluded volume forces has been studied in earlier work[55–57,60,80] but the new feature of Fig. 3(a) is that the behavior is almost universal. Only on magnified scales (inset of Fig. 3(a)) can one distinguish that the continuum model data and the lattice model data settle down on two distinct parallel straight lines for $L/\ell_p > 10$. In fact, for $L \gg \ell_p$ we expect a behavior typical for SAW's in $d = 2$, namely,

$$\langle R_N^2 \rangle = A\ell_p^{1/2}L^{3/2}, \quad L \gg \ell_p, \tag{14}$$

where the dimensionless amplitude factor A is a nonuniversal constant. Fig. 3(b) hence presents a plot of $\langle R_N^2 \rangle/(2L\ell_p(L/\ell_p)^{1/2})$ which shows in more detail how the limiting behavior of Eq. (14) is approached. One can see that in the crossover region

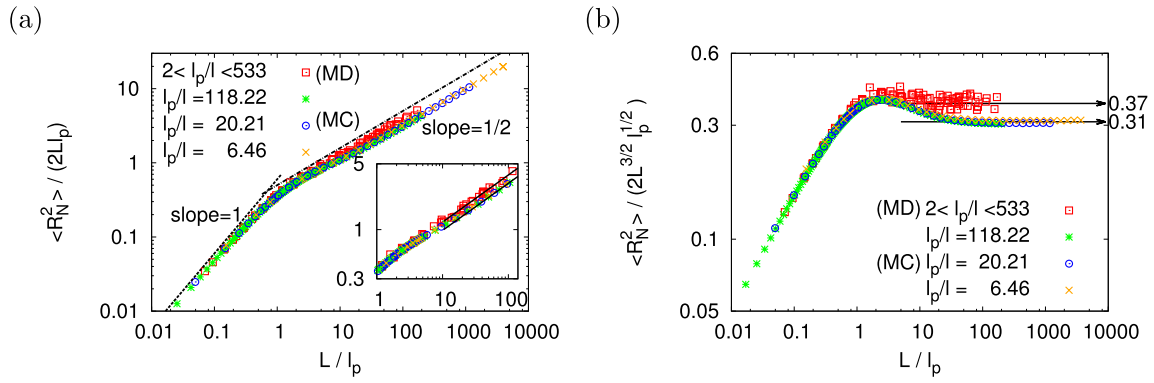

FIG. 3. (a) Log-log plot of $\langle R_N^2 \rangle/(2L\ell_p)$ as a function of L/ℓ_p, combining the result of both MC and MD simulations, for the models of Sec. II. MC data include many chain lengths up to $N = 25\,600$, for three choices of the stiffness: $\ell_p/\ell = 6.46$ ($q_b = 0.1$), 20.21 ($q_b = 0.03$), and 118.22 ($q_b = 0.005$), respectively. MD data[80] (indicated as squares) are for $16 \le N \le 2048$, with $0 \le \kappa \le 320$ ($\ell_p/l \approx 1.66\kappa$). The dashed and dotted-dashed lines indicate the rod regime and the excluded volume power law, respectively. No adjustable parameters whatsoever have been used in this plot. The inset shows the same data in the range from $1 < L/\ell_p < 140$, and separate straight lines were fitted to the data from MD and MC for $L/\ell_p > 10$, respectively. (b) Log-log plot of the dimensionless ratio $\langle R_N^2 \rangle/(2L^{3/2}\ell_p^{1/2})$ versus L/ℓ_p, using the same (non-universal!) amplitude factors $A/2 = 0.31$ for the lattice model and $A/2 = 0.37$ for the continuum model, respectively. Note that statistical errors of the MC data are smaller than the size of the symbols throughout. In (b), statistical errors of the MD data are almost twice the size of the squares, for $L > \ell_p$, but not shown for the sake of clarity.

between rods and SAW's, namely, for $1 \le L/\ell_p \le 10$, there occurs some overshoot, and this overshoot is more pronounced for the lattice model than for the continuum model. Of course, this behavior in the crossover region is quite nontrivial, and there is no simple interpretation by scaling arguments known.

Next we consider transverse fluctuations of the semiflexible chains. For this purpose we introduce an instantaneous coordinate system (ξ,η) for each configuration of the chain such that the ξ-axis is oriented along the end-to-end vector of the chain, so $\hat{\xi} = \vec{R}_N/|\vec{R}_N|$ is a unit vector along the ξ direction. We then define the transverse fluctuations as

$$\ell_\perp^2 = \frac{1}{N}\sum_{i=1}^{N} \eta_i^2, \tag{15}$$

with (ξ_i,η_i) being the coordinates of the ith monomer in this (ξ,η) coordinate system. Fig. 4 then presents a plot of $\langle \ell_\perp^2\rangle^{1/2}/L$ versus L/ℓ_p. In the rod regime, it is well-known[15,88,89] that

$$\langle \ell_\perp^2\rangle \propto L^3/\ell_p, \quad L \ll \ell_p, \tag{16}$$

while for $L \gg \ell_p$, the configuration of the chain simply is a swollen coil, and the direction of $\hat{\xi}$ does no longer play a special role: so we expect $\langle \ell_\perp^2\rangle = A' \ell_p^{1/2} L^{3/2}$, compare with Eq. (14), where A' is another amplitude factor. Hence, $\langle \ell_\perp^2\rangle^{1/2}/L = (A')^{1/2}(\ell_p/L)^{1/4}$ in this limit, and this is what we see in Fig. 4. The result that Eq. (16) also applies to the lattice chains is rather unexpected, of course, since on the lattice for $L \ll \ell_p$ typical configurations have either no kink at all on the length L or exhibit a single kink (the walk goes straight along a lattice direction for L' steps and then L'' steps in the direction perpendicular to the direction of the first L' steps with $L = L' + L''$, while walks with two or more kinks make negligible contributions). Figs. 3 and 4 hence reveal that the average geometrical properties of semiflexible polymers depend only very little on the model used to describe them, lattice and continuum models exhibit almost no difference, although the actual conformations are very different.

We also suggest that a plot of experimental data of $\ln(\langle \ell_\perp\rangle^{1/2}/L)$ versus $\ln(L/\ell)$ would be a good way to obtain an estimate for the persistence length ℓ_p, since the maximum of this curve (Fig. 4) seems to occur for $\ln(L/\ell_p) = 1$, i.e., $\ln(L/\ell) = 1 + \ln(\ell_p/\ell)$. This analysis, applied to atomic force microscope (AFM) images of DNA chains (as are available

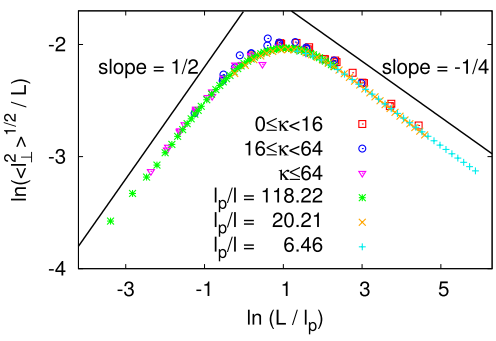

FIG. 4. Logarithm of the scaled transverse fluctuation $\langle \ell_\perp^2\rangle^{1/2}/L$ as a function of $\ln(L/\ell_p)$ with data of both MC and MD for various choices of the persistence length listed in Table I, as indicated. The asymptotic power laws $\langle \ell_\perp^2\rangle^{1/2}/L \propto (L/\ell_p)^{1/2}$ for $L < \ell_p$ and $\langle \ell_\perp^2\rangle^{1/2}/L \propto (L/\ell_p)^{-1/4}$ for $L > \ell_p$ are indicated by solid straight lines.

in the literature[90,91]), may be an interesting alternative to the traditional fitting of the Kratky-Porod results, Eq. (13), to the chain linear dimensions of such semiflexible polymers adsorbed to substrates. Since Eq. (13) breaks down in $d = 2$, for $L \gg \ell_p$, use of Eq. (13) may lead to significant systematic errors.

IV. SEMIFLEXIBLE POLYMERS CONFINED IN A SLIT WITH REPULSIVE BOUNDARIES

We now study semiflexible polymers in quasi-one-dimensional confinement, extending the discussions that were already given in our preliminary work.[34,36] The considered lattice model is defined in Fig. 2(c), and the continuum model (sketched in Fig. 2(b)) is defined precisely by Eqs. (6)–(10).

In computer simulations of very long polymer chains in confinement, a crucial question is whether the statistical effort invested is large enough so that the configuration space of the model is sampled sufficiently well. This problem is a serious concern both for the PERM Monte Carlo algorithm (when the coarse-grained free energy function of the model splits into distinct "valleys" separated by entropic barriers, one must make sure that all "valleys" are properly sampled[50]) and for MD. In MD, we expect very long relaxation time to form hairpins [Fig. 2(a)] and to equilibrate them; it might occur that hairpins form primarily at the free chain ends and then diffuse along the contour of the chain towards its center.

To clarify such problems, we have recorded time sequences of snapshot pictures of the chain configurations for representative choices of parameters. Fig. 5(a) (Multimedia view) gives a few typical examples. One can see that at the first time (t = 527), there is no hairpin, at the second time (t = 886), there is a hairpin at the rightmost part of the chain and another one in the central part of the chain, and at the third picture (t = 1456), all these structures are gone, and a double hairpin configuration (similar to the qualitative sketch in Fig. 2(a)) near the left end of the chain has formed. At a still later time (t = 1700), a state with no hairpin is found again. Thus, one can see that (for the chosen parameters) hairpins are quickly formed and relax again, the "lifetime" of hairpins being small in comparison to the length of the MD run. For the chosen parameters the polymer neither resembles a string of blobs nor a flexible rod, but takes intermediate types of states. For $D \ll \ell_p$ (Figs. 5(b) and 5(c) (Multimedia view)), one finds in practice never any configurations with hairpins, the latter occur typically when $\ell_p \le D \le 3\ell_p$, while for still wider strips, the "string of blobs" picture starts to apply. However, for the choice $D = 80$, $\ell_p = 3.30\ell$ shown in Fig. 5(b) (Multimedia view), the chain of length $N = 1024$ is merely long enough to form 2-3 blobs only. From the snapshots, it also is evident that monomers occur near the walls occasionally, but much more frequently they are near the center of the strip.

Fig. 5 (Multimedia view) does display some qualitative similarity to the description proposed by Odijk[15] who introduced for the case $D < \ell_p$ the concept of the deflection length, Eq. (1), see also Fig. 2(a), using the Kratky-Porod model, Eq. (2). It is an interesting issue to examine to what extent our simulations confirm this description quantitatively.

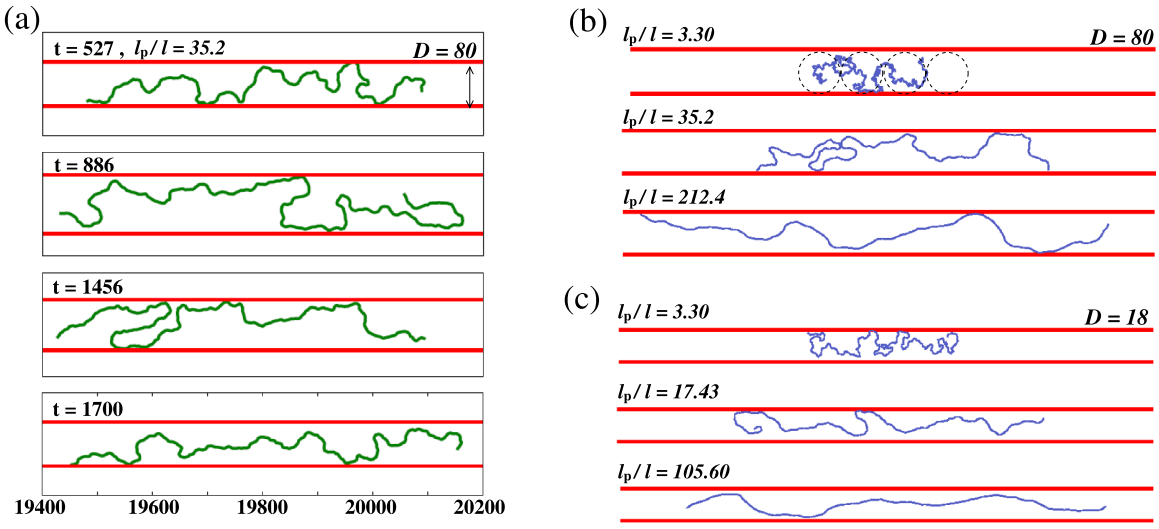

FIG. 5. (a) Selected snapshots from the MD simulation for $N = 1024$ $D = 80$, $\ell_p = 35.2\ell$ (i.e., the choice $\kappa = 21.6$) at various times (the time of the snapshots is the number in the left upper corner of the snapshot, given in units of 5000 MD time units, times $t = 527$, 886, 1456, and 1700 being shown). Note that the resolution of the snapshot is not high enough to display the individual effective monomers of the simulated model (at high resolution, the snapshots would resemble Fig. 2(b)). Note that the x and y axes are plotted with equal length scale, avoiding any distortion between the length in x and y directions. The solid straight lines represent the two boundaries of the strip. (b) Snapshots for chains with $N = 1024$ for $D = 80$ and three choices of persistence length, $\ell_p = 3.30\ell$, 35.2ℓ, and 212.4ℓ, as indicated. (c) Snapshots for chains with $N = 256$ for $D = 18$ and three choices of persistence length, $\ell_p = 3.30\ell$, 17.43ℓ, and 105.60ℓ, as indicated. Movies shown online are made with visual molecular dynamics (VMD).[51] (Multimedia view) [URL: http://dx.doi.org/10.1063/1.4929600.1] [URL: http://dx.doi.org/10.1063/1.4929600.2] [URL: http://dx.doi.org/10.1063/1.4929600.3] [URL: http://dx.doi.org/10.1063/1.4929600.4] [URL: http://dx.doi.org/10.1063/1.4929600.5] [URL: http://dx.doi.org/10.1063/1.4929600.6]

A naive analysis of the configurations can be based on a study of the local angle ϕ_i of the bond between monomers i and $i + 1$ and the x-axis, and search for the locations of local maxima of $\cos\phi_i$ along the chain contour: in the (x, y)-plane these local maxima correspond to extrema of the curve that is generated by connecting the discrete points (x_i, y_i) making the monomer positions along the chain (Fig. 6(a)). The distance between subsequent extrema could be taken as a first estimate of the deflection length λ.

However, little thoughts reveal that such a procedure would be quite misleading: the bond angles θ_i between subsequent bonds due to thermal fluctuations have random values

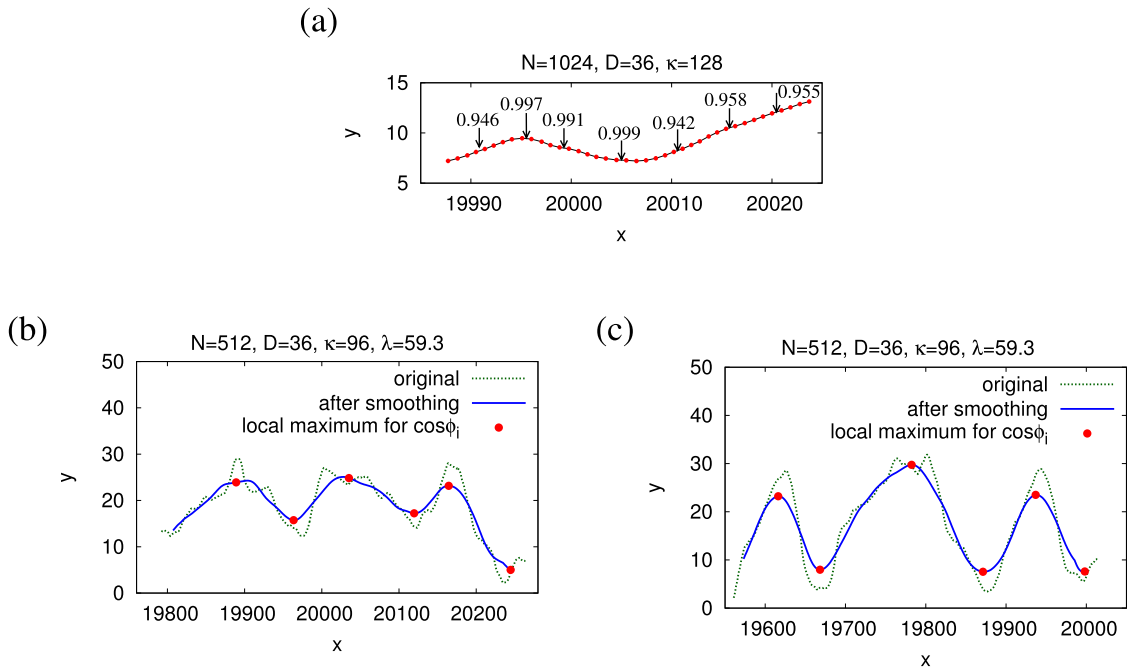

FIG. 6. (a) Plot of a small part of a typical configuration of a chain with $N = 1024$ monomers for the case $D = 36$, $\kappa = 128$. Each solid dot indicates the (x, y) coordinates of a monomer: note that the lengths in x and y directions are plotted with equal scale. The arrows show selected values of $\cos\phi_i$: for the shown "wiggle" from the maximum with $\cos\phi_i = 0.997$ to the next minimum of the contour with $\cos\phi_i = 0.999$, only 10 monomers occur, but $\Delta y \approx 2$ (see text). (b) and (c) Comparison of two configurations after smoothing (full curves) to their corresponding original unsmoothed configurations (broken curves) for the case $N = 512$, $D = 36$, and $\kappa = 96$. Note that here the scale for the x-axis is compressed in comparison to the scale for the y-axis by a factor of 6. The dots show the "deflection points" that are kept for the measurement of $P(\lambda)$, λ being the distance between neighboring deflection points.

of order $\pm\sqrt{k_BT/\kappa}$ (equipartition theorem). Adding up such random increments gives rise to "wiggles" in the chain configurations on many length scales. Of course, the discreteness of the chain provides a small scale cutoff, and we need to average of the order of 10 subsequent monomers to obtain this random walk-like behavior of the angular increments, but such small scale wiggles create a displacement Δy in y-direction which is of order unity only, not of order D. The deflection length, however, is intended to rather measure the length scale of wiggles in the chain configurations, with displacement of order D.

In order to measure this large scale, we have to construct a coarse-grained configuration. A practically useful prescription is to apply a coordinate smoothing procedure

$$\overline{x_i} = (2m+1)^{-1} \sum_{j=i-m}^{i+m} x_j, \qquad \overline{y_i} = (2m+1)^{-1} \sum_{j=i-m}^{i+m} y_j. \quad (17)$$

We have found that for persistence lengths of the order of 100, a value of $m = 31$ yielded satisfactory results, smoothing out the small scale wiggles but leaving the large scale configuration of the chain intact (Figs. 6(b) and 6(c)). Of course, there is still the problem that near an extremum of the coarse-grained curve, ϕ_i changes its sign many times, leading to several close by extrema of $\cos\phi_i$. For automatic detection of local maxima for $\cos\phi_i$, only sites i that satisfy $\cos\phi_i > c$ were considered (with a threshold value $c = 0.998$ if the persistence length is of order 100, i.e., $|\phi_i| \approx 4°$), and among the "deflection" sites thus found only those are kept, which are more distant from each other than a distance $d = \lambda/3$ where λ is the Odijk result, Eq. (1). These remaining extrema are indeed the desired deflection points of the coarse-grained configuration where the distance Δy in y-direction from one deflection point to the next one is much larger than unity (Figs. 6(b) and 6(c)). From this coarse-graining procedure, we obtain estimates for both the average deflection length $\bar{\lambda}$ and the width $\Delta\lambda$ of the distribution function $P(\lambda)$, see Table II. It is seen that the results are of the same order as Eq. (1); of course, in Eq. (1), a prefactor of order unity is suppressed, as always in scaling arguments, and hence perfect agreement cannot be expected. The fact that $\Delta\lambda$ and $\bar{\lambda}$ are of the same order reflects the irregularity of the chain configurations, expected from entropic reasons.

TABLE II. Selected estimates for the deflection length.

N	D	κ	λ (Eq. (1))	$\bar{\lambda}$	$\Delta\lambda$
512	36	96	59.3	76.2	28.5
1024	36	128	65.2	85.0	30.9
1024	80	128	111.0	102.4	43.9

The first question to ask is whether or not confinement leads to a change of the local persistence length (which we always define from Eq. (5)). Fig. 7 shows the unexpected result that the persistence length $\ell_p(D)$ does depend strongly on the strip width D for the lattice model when D is less than the persistence length of the unconfined chain in the bulk ($\ell_p^{\text{bulk}} = \ell_p(D \to \infty)$), while for the off-lattice model, ℓ_p remains completely unaffected by the confinement. When we henceforth use ℓ_p without any further specification, always the bulk value will be meant. This finding implies for the continuum model that the average orientational correlation between subsequent bonds (as measured by $\langle\cos\theta\rangle$) is the same for the confined chains as it is in the bulk, although for small D (and in the absence of hairpins), all bond vectors of the confined chains are oriented almost parallel to the x-axis, while for semiflexible polymers in the bulk, this dominance of one orientation does not occur. For off-lattice semiflexible chains, we have $\langle\theta^2\rangle \approx \ell/\ell_p$ and if $D \ll \ell_p$ we can expect that after $n_\lambda = \lambda/\ell$ steps along the chain, the angle $\theta(n_\lambda)$ has added up in a random walk-like fashion,[15] i.e., $\langle[\theta(n_\lambda)]^2\rangle = n_\lambda\ell/\ell_p = \lambda/\ell_p$. However, this growth of $\langle[\theta(n_\lambda)]^2\rangle$ must stop when $\langle[\theta(n_\lambda)]^2\rangle = (D/\lambda)^2$, and equating both expressions readily yields the deflection length,[15] Eq. (1). The different behavior of the lattice model can be interpreted by the fact that the typical configuration of the chain (Fig. 1(c)) consists of a sequence of kinks, where at each kink point a sequence of n_x bonds in x-direction is followed by n_y bonds in y-direction. The numbers of n_x, n_y follow an exponential distribution[57]

$$P(n_x, n_y) = \left(\frac{\ell}{\ell_p}\right)^2 \exp(-n_x\ell/\ell_p)\exp(-n_y\ell/\ell_p). \quad (18)$$

In a bulk square lattice, both n_x and n_y can vary from 1 to infinity. For large ℓ_p/ℓ, the average length of a sequence can

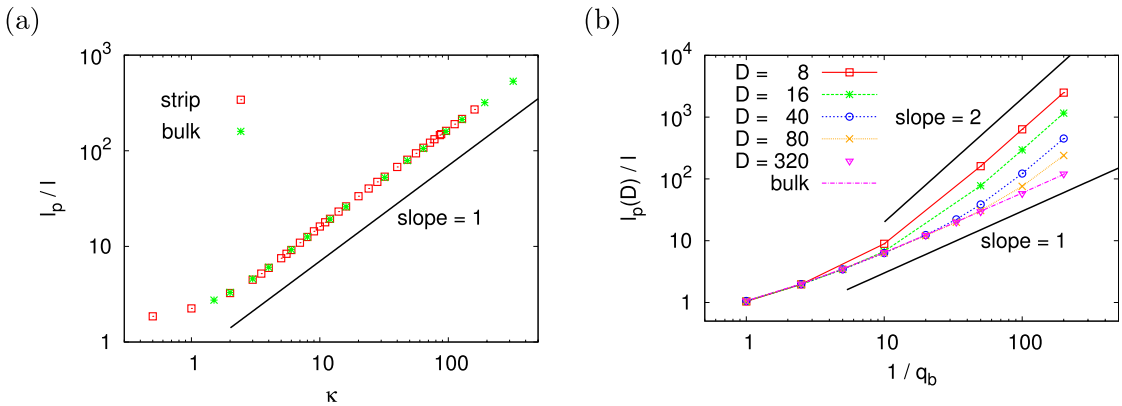

FIG. 7. Comparison of the persistence length ℓ_p/ℓ under confinement in a strip and in the bulk for the continuum model (a) and for the lattice model, using strip widths from $D = 8$ to $D = 320$ (b). Note that the estimates of persistence length under confinement in (a) were obtained by taking the average of $\ell_p(D)$ for several choices of D at fixed κ. Note that error bars in this plot are smaller than the size of the symbols throughout.

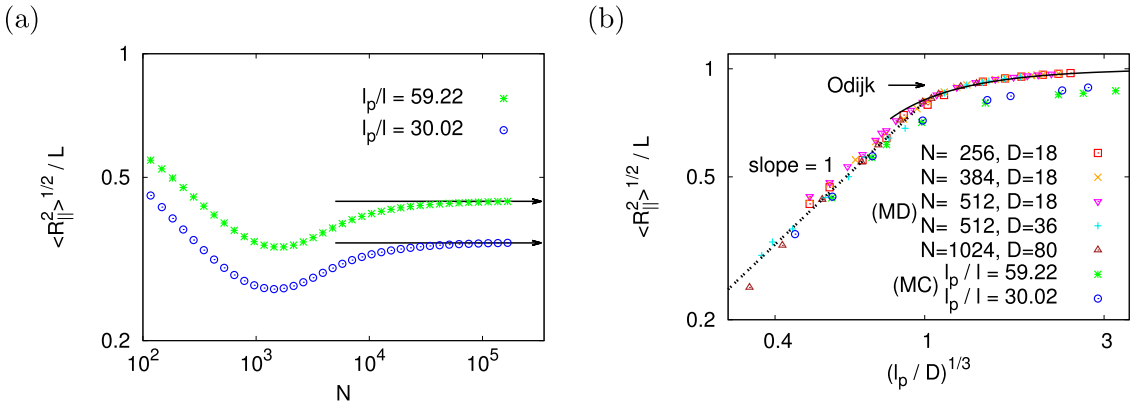

FIG. 8. (a) MC data for $\langle R_{\|}^2 \rangle^{1/2}/L$ plotted vs. chain length N, for $D = 320$, and two choices of the persistence length, $\ell_p/\ell = 59.22$ ($q_b = 0.01$) and $\ell_p/\ell = 30.02$ ($q_b = 0.02$), respectively. The solid horizontal lines indicate the extrapolation towards $N \to \infty$. (b) Log-log plot of the dimensionless chain extension $\langle R_{\|}^2 \rangle^{1/2}/L$ versus the ratio $(\ell_p/D)^{1/3}$ for data from both MD and MC. The dashed straight line indicates the De Gennes regime for $D > \ell_p$, $\langle R_{\|}^2 \rangle^{1/2} \propto L(\ell_p/D)^{1/3}$. The solid line shows a fit of the MD data to the Odijk prediction. Note that the MC data were all extrapolated towards $N \to \infty$, as shown in part (a), while the MD data refer to specific values of N in the range $256 \le N \le 1024$ for $D = 18, 36$, and 80, as indicated. Statistical errors are at most of the size of the symbols.

be computed simply as

$$\langle n_x \rangle = \int_0^\infty dn_x \int_0^\infty dn_y \, n_x P(n_x, n_y) = \ell_p/\ell, \text{ unconfined case,} \tag{19}$$

and the same result would be obtained for $\langle n_y \rangle$, since in the bulk both lattice directions are equivalent. However, for the confined system, n_y must be in the range $1, \ldots, n_y, \ldots, D$ (Fig. 2(c)). While Eq. (18) implies that a kink with some choice of (n_x, n_y) occurs with probability unity, for the confined system Eq. (18) allows for the occurrence of a kink only with the reduced probability $P_{\text{kink}} = 1 - \exp(-D/\ell_p)$. This reduction in the number of kinks must show up in the distance between subsequent kinks along the x-direction, and hence, we tentatively suggest

$$\langle n_x \rangle = (\ell_p/\ell)/P_{\text{kink}} = (\ell_p/\ell)/[1 - \exp(-D/\ell_p)]. \tag{20}$$

The data of Fig. 7(b) are indeed compatible with this simple argument, implying that for $D < \ell_p$, the effective persistence length[34] $\ell_p(D) \equiv \langle n_x \rangle \ell \approx \ell_p^2/D$. Hence for $D < \ell_p$ in the case of the lattice model, it will matter whether we study the behavior of the chain linear dimensions as a function of ℓ_p/D or $\ell_p(D)/D$, respectively. For simplicity, in this discussion we have ignored the possible effect of hairpins completely (note that when hairpins occur and the end-to-end vector is oriented from left to right, numbers n_x of sequences parallel and antiparallel to the x-component of the end-to-end vector are not equivalent).

We first demonstrate that the possible renormalization of the persistence length does not matter when we study the regime where the Daoud-De Gennes[40] prediction applies (Fig. 8),

$$\langle R_{\|}^2 \rangle^{1/2} \propto (\ell_p/D)^{1/3} L. \tag{21}$$

From the MC calculation, data for a very wide range of N are available, and hence for each choice of D and ℓ_p, one can perform an extrapolation to $N \to \infty$. Since the variation of $\langle R_{\|}^2 \rangle^{1/2}/L$ with N is non-monotonic (Fig. 8(a)), such a procedure would be completely misleading if only data for rather short chains (on the left side of minimum) were available. Thus, no such extrapolation was attempted for the MD data, but nevertheless a reasonable scaling could be obtained (Fig. 8(b)). We note that the nonmonotonic variation of Fig. 8(a) is not specific for the lattice model; a similar behavior was also found for a chain of tangent hard spheres.[37] The location of this minimum of the ratio $\langle R_{\|}^2 \rangle^{1/2}/L$ depends on both D and ℓ_p, as demonstrated in our earlier work.[34] It is seen that the lattice

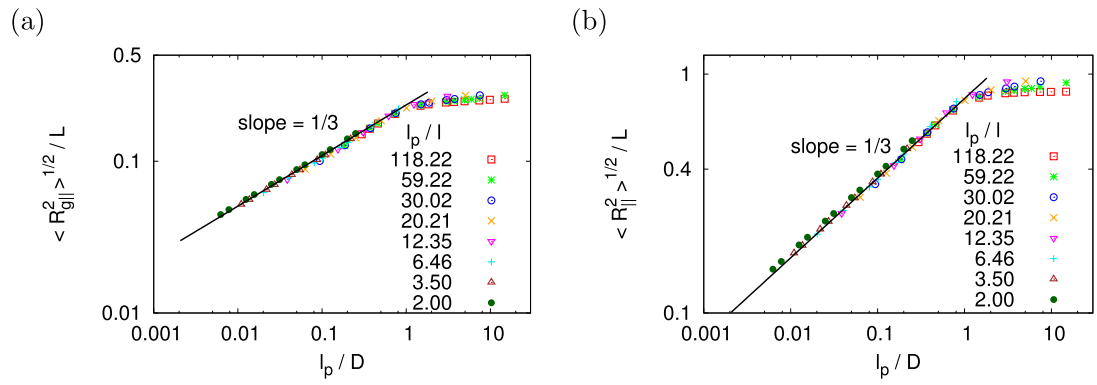

FIG. 9. Log-log plot of $\langle R_{g\|}^2 \rangle^{1/2}/L$ (a) and $\langle R_{\|}^2 \rangle^{1/2}/L$ (b) versus ℓ_p/D. Various values of q_b are shown, as indicated. Note that all these data were obtained by first extrapolating the data for finite L (see Fig. 8(a)) at fixed q_b and fixed D towards $L \to \infty$.

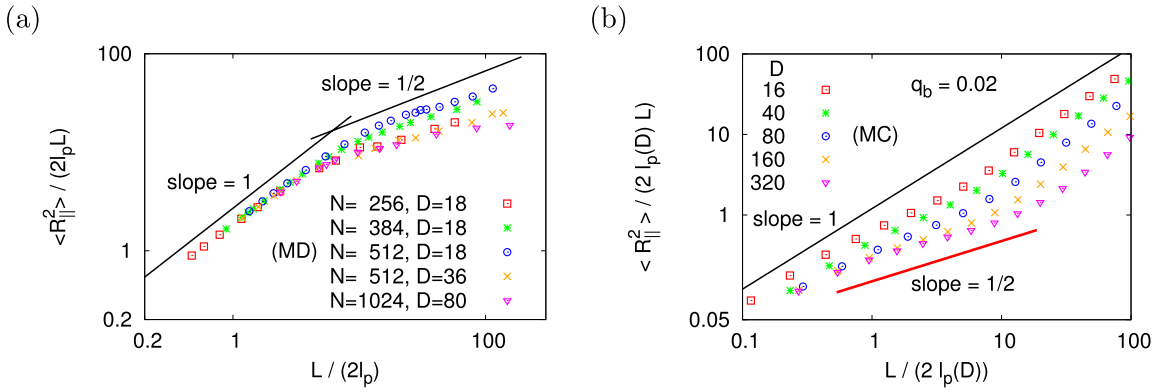

FIG. 10. Log-log plot of $\langle R_\parallel^2\rangle/(2\ell_p L)$ (a) or $\langle R_\parallel^2\rangle/(2\ell_p(D)L)$ (b), versus $L/(2\ell_p)$ or $L/(2\ell_p(D))$, respectively. For the MD data, both L, D, and ℓ_p were varied, as indicated in the key to the figure. For the MC data, the choice $q_b = 0.02$ (i.e., $\ell_p = 30.02\ell$) was fixed and L was varied, showing five different choices of D, as indicated.

and off-lattice models yield a qualitatively similar behavior, the constant of proportionality in Eq. (21) is somewhat smaller for the lattice model, and also the approach to saturation in the limit of strong confinement ($\ell_p/D \gg 1$) is much slower. In view of the fact that for the lattice model in the regime $\ell_p > D$, the persistence length gets renormalized to much larger values, it may seem paradoxical that nevertheless the scaled chain extension $\langle R_\parallel^2\rangle^{1/2}/L$ is smaller than in the continuum case. However, the explanation of this behavior is that those parts of the chain that are oriented along the y-axis (Fig. 2(c)) do not contribute to the extension in x-direction at all, while in the continuum case the angles ϕ_i due to the weak deflections all are rather small and hence all bonds contribute predominantly to the chain extension along the x-axis. In fact, as we shall see later, in the lattice model monomers are less repelled by the confining boundaries than in the continuum case (compare the density profiles across the slit in Figs. 12(a) and 13(a)).

In the lattice model, both the mean square radius $\langle R_\parallel^2\rangle$ and the mean square gyration radius $\langle R_{g\parallel}^2\rangle$ in x-direction have been obtained for a wide range of choices of both D and the persistence length ℓ_p, and display the expected scaling as a function of ℓ_p/D very well (Fig. 9), in the limit of very long chains. We stress that for the MC data in Figs. 8(b) and 9, the unrenormalized values of ℓ_p (i.e., the persistence length of the unconfined chains in the bulk) were used in the variables $(\ell_p/D)^{1/3}$ or ℓ_p/D, respectively. However, if we use $\ell_p(D)/D$ rather than ℓ_p/D for such plots, they look very similar: this happens because $\ell_p(D)/D$ differs from ℓ_p/D only for $\ell_p/D > 1$ and in this region the scaling functions in Figs. 8(b) and 9 are almost flat.

Next we discuss the variation of the linear dimension with chain length, normalizing $\langle R_\parallel^2\rangle$ by the Kratky-Porod prediction $2\ell_p L$, and measure the contour length L in units of the Kuhn length $2\ell_p$ (Fig. 10). There are three regimes: for $L/(2\ell_p) < 1$, the chains behave like rods, $\langle R_\parallel^2\rangle = L^2$ and hence $\langle R_\parallel^2\rangle/(2\ell_p L) = (L/\ell_p)/2$, the first linear regime in the log-log plot. For wide strips ($D \gg \ell_p$), there is an intermediate regime, where the chain behaves like a weakly constrained free chain [Eq. (14)], and hence $\langle R_\parallel^2\rangle/(2\ell_p L)$ varies like $(L/\ell_p)^{1/2}$. For narrow strips (such as the case $D = 16$, $\ell_p = 30.02\ell$ in Fig. 10(b)), this regime is absent, of course. For the MD data in Fig. 10(a), this regime is realized by choosing not so large values of ℓ_p, since extremely large values of N are not accessible. The MC data show a third regime where $\langle R_\parallel^2\rangle/(2\ell_p(D)L)$ again varies linearly with $L/(2\ell_p(D))$, which simply is the Daoud-De Gennes regime again (where the chain is a string of blobs). For the rather wide strip used for the MD data, this regime cannot be recognized yet in Fig. 10(a). When we study the regime $D < \ell_p$ for the lattice model and consider the crossovers with increasing L, it is the renormalized persistence length $\ell_p(D)$ which matters for the crossover to the final regime $\langle R_\parallel^2\rangle \propto L^2$ for large L. Therefore, we used $\ell_p(D)$ in Fig. 10(b).

At the first glance, Fig. 10 seems at variance with Fig. 8, since from the MD data plotted there no evidence for the string of blobs-picture of Daoud and De Gennes[40] was seen. However, this is not the case: when we plot $\langle R_\parallel^2\rangle/(\ell_p^{1/2}L^{3/2})$ versus the effective number $L/L_{\rm cross}$ of blobs in the string (Fig. 11), we find that a significant part of the MD data falls in the range $4 < L/L_{\rm cross} < 30$ and roughly is consistent with Eq. (21), which in this representation can be rewritten as

$$\langle R_\parallel^2\rangle/(\ell_p^{1/2}L^{3/2}) \propto (L/\ell_p)^{1/2}(\ell_p/D)^{2/3} = (L\ell_p^{1/3}/D^{4/3})^{1/2}. \tag{22}$$

Of course, the MC data include a much wider range of $L/L_{\rm cross}$, including the chains that are almost unperturbed by the confinement ($L/L_{\rm cross} < 1$, then $\langle R_\parallel^2\rangle/(\ell_p^{1/2}L^{3/2})$ is essentially constant), as well as very long chains (where $L/L_{\rm cross} > 100$).

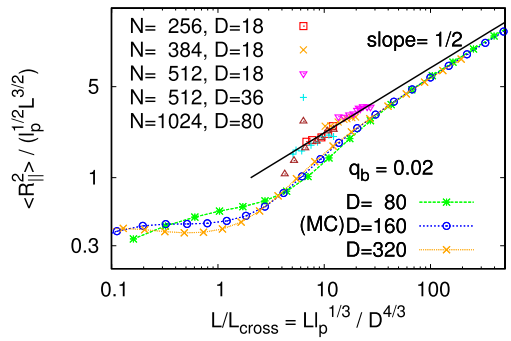

FIG. 11. Log-log plot of $\langle R_\parallel^2\rangle/(\ell_p^{1/2}L^{3/2})$ versus $L/L_{cross} = L\ell_p^{1/3}/D^{4/3}$ including both the MD and MC data. Note that $L_{\rm cross}$ denotes the contour length where the crossover from the unconfined SAW to the string of Daoud-De Gennes blobs occurs (so $L/L_{\rm cross}$ is essentially the number of blobs). The straight line illustrates Eq. (22).

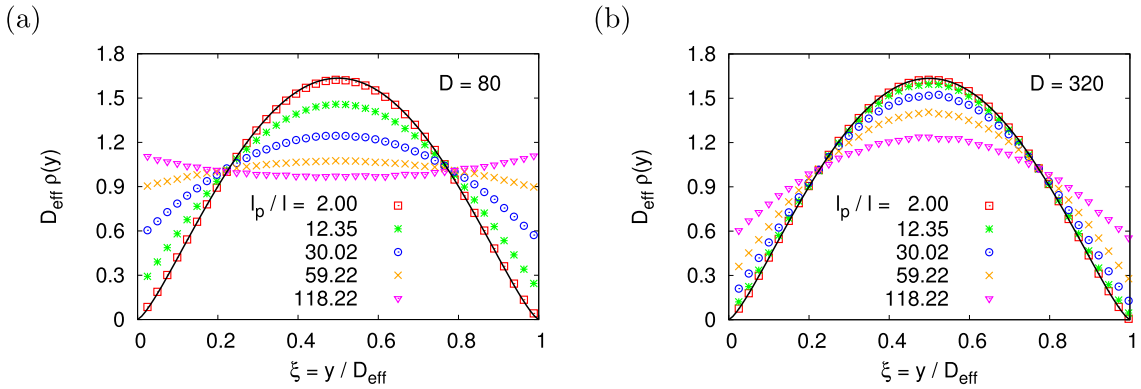

FIG. 12. Rescaled monomer density profile $D_{\rm eff}\rho(y)$ versus $\xi = y/D_{\rm eff}$ for the case $D = 80$ (a) and $D = 320$ (b), according to the MC model. Several choices of ℓ_p/ℓ are included, as indicated. Full curves show the theoretical prediction, Eq. (23), with the constant C fitted as $C = 10.38$. Here, $D_{\rm eff} = D + 1$.

A very interesting aspect is the monomer density profile near the wall. For flexible chains, it was shown[46] that for the lattice model this profile can be very accurately described by

$$D_{\rm eff}\rho(y) = C[\xi(1-\xi)]^{4/3}, \quad \xi = y/D_{\rm eff}, \tag{23}$$

where $D_{\rm eff} = D + 1$. This form is compatible with the density profile expected for a semi-infinite solution (with density ρ_b in the bulk) of flexible chains near a hard wall,[92,93]

$$\rho(y) = \rho_b \tilde{\rho}(y/R), \quad R \approx \ell(L/\ell)^{\nu}, \tag{24}$$

with $\nu = 3/4$ in $d = 2$ dimensions, and $\tilde{\rho}(\xi) \propto \xi^{1/\nu}$ for $\xi \ll 1$. However, Semenov[77] predicted on the basis of the Kratky-Porod model that

$$\rho(y)/\rho_b \propto y^{2/3} \quad \text{for} \quad \ell \ll y \ll \ell_p, \tag{25}$$

irrespective of dimensionality. However, the data for the lattice model do not yield any evidence in favor of this prediction (Fig. 12).

For the off-lattice case the conclusion is different; however, the monomer density near the walls does not extrapolate to a nonzero value when $\xi = y/D_{\rm eff} \to 0$ or $\to 1$, Fig. 13(a), and when ℓ_p is large, Eq. (23) then no longer provides a good fit of the data. Thus, it is tempting to try a log-log plot of $\rho(y)$ versus y. Of course, data for $y > D/4$ are affected by the saturation of the profile in the center of the film and have to be excluded (one should only use data far outside the range of the repulsive wall potential). One sees that in the intermediate regime, the MD data indeed are consistent with a crossover of the "effective exponent," defined in terms of the apparent slope where a straight line can be fitted to the data of the log-log plot near $y \approx 10$ from 4/3 (for flexible chains) to 2/3 (for very stiff chains). This finding hence is compatible with Semenov's prediction, Eq. (25). Here, the possibility of small bond angles implicit in the Kratky-Porod model is a crucial feature, and hence, it is not so surprising that for the lattice model Eq. (25) does not hold. Of course, very close to the wall the actual wall potential matters, and hence, the power laws are expected to hold only for $y \gg \ell$, see Eq. (25).

Very interesting is also the behavior of the end monomer distribution $\rho_e(y)$. For flexible chains, the scaling prediction is[46]

$$\rho_e(y) = \frac{1}{D_{\rm eff}} C_e[\xi(1-\xi)]^{25/48}, \tag{26}$$

and indeed this (empirical) function provides a very good fit of the MD data for flexible chains ($\kappa = 0$), with the constant $C_e \approx 2.71$ being of the same order as for the SAW model on the square lattice[46] ($C_e = 2.85$). Again one sees that with increasing stiffness, the end monomer density near the walls gets enhanced, and for very stiff chains a limiting behavior

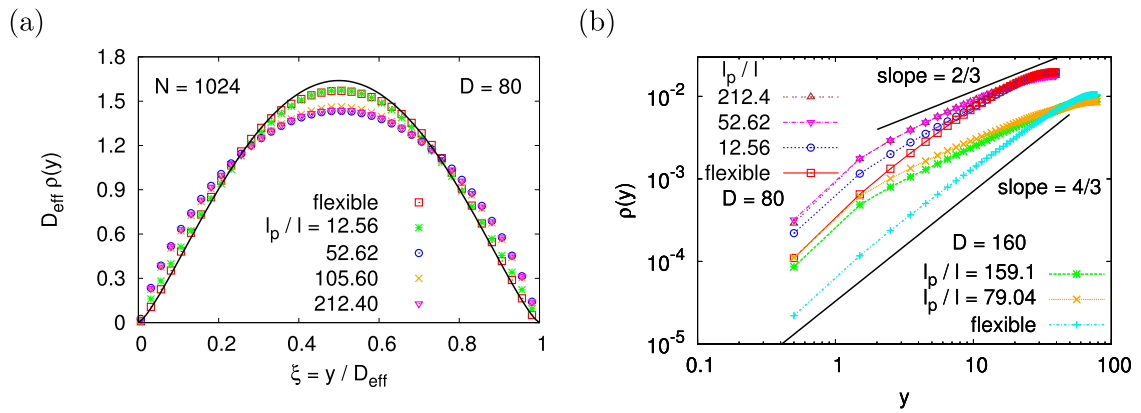

FIG. 13. (a) Plot of the scaled monomer density $D_{\rm eff}\rho(y)$ as a function of $\xi = y/D_{\rm eff}$ for the continuum model of semiflexible chains with $N = 1024$, as obtained from MD simulations, for a strip of width $D_{\rm eff} = D = 80$, and several choices of the persistence length ℓ_p/ℓ, as indicated. The solid curve shows the fit to Eq. (23) for the fully flexible case, with the constant C being $C = 10.41$. (b) Log-log plot of the monomer density $\rho(y)$ versus y for $N = 1024$, $D = 80$ and 160, and various stiffnesses as indicated by the choices for ℓ_p/ℓ. The solid straight lines indicate the theoretical power laws $\rho(y) \propto y^{4/3}$ for the flexible and $\rho(y) \propto y^{2/3}$ for Kratky-Porod chains, respectively.

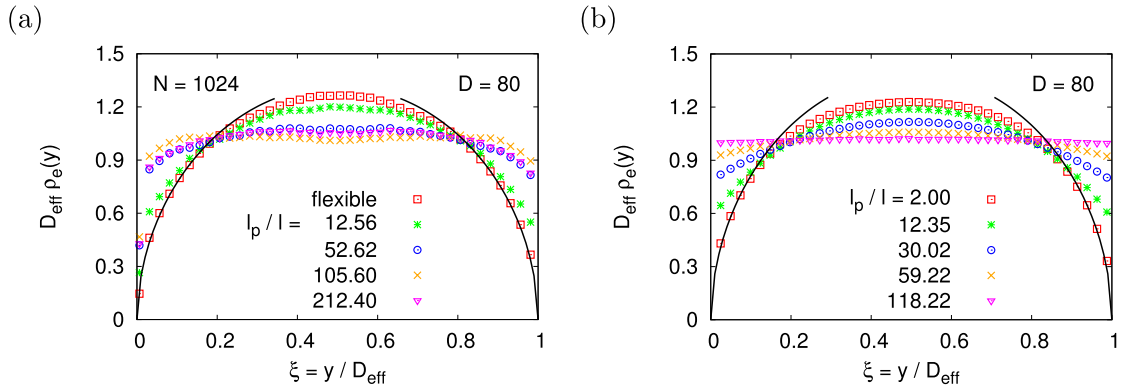

FIG. 14. Scaled end monomer density profiles $\rho_e(\xi)D_{\text{eff}}$ as a function of $\xi = y/D_{\text{eff}}$ for the continuum model of semiflexible chains with $N = 1024$, as obtained from MD simulations (a), and for the lattice model of chains with $50\,000 < N < 200\,000$ (b). Note that $D_{\text{eff}} = D$ was chosen for the off-lattice model but $D_{\text{eff}} = D + 1$ for the lattice model, and several choices of the persistence length are shown as indicated. The full curve shows a fit of Eq. (26) for the fully flexible case, with the constant C_e being $C_e = 2.71$ for the continuum, and $C_e = 2.85$ for the lattice.

$\rho_e(y) \approx const$ seems to be reached (apart from a small region $\xi < 0.1$ or $1 - \xi < 0.1$, where ρ_e is slightly depressed, but this could be a residual effect from the nonzero range of the repulsive wall potentials). Thus, we speculate that for semiflexible chains (in the limit $N \to \infty$ and then $\ell_p \to \infty$ in a semi-infinite dilute solution), there is no analogue of the power law for the monomer density, Eq. (25), when one considers the density of end monomers instead. In the lattice model, also an essentially constant distribution of $\rho_e(y)$ across the strip was found (Fig. 14(b)). While in the regime $D_{\text{eff}} < \ell_p$ the behavior of $\rho(y)$ and $\rho_e(y)$ for the lattice model is very similar, this is not true for the bead-spring model of semiflexible chains in the continuum.

V. CONCLUSIONS

We now proceed by summarizing the central findings of the present work. We have simulated two rather different coarse-grained models of semiflexible polymers in two space dimensions, over a wide range of chain lengths and persistence lengths, under good solvent conditions, both in the bulk and under confinement in a strip of width D with repulsive boundaries. One model is a self-avoiding walk on the square lattice, where stiffness is controlled by the energy cost ϵ_b if the walk makes a kink of ±90°. The density of the kinks for large ϵ_b/k_BT decreases exponentially with this energy cost, proportional to $\exp(-\epsilon_b/k_BT)$, and the persistence length ℓ_p then is essentially the inverse of the kink density, $\ell_p \propto \exp(\epsilon_b/k_BT)$, and can also be interpreted as the average length of straight sequences of bonds between two neighboring kinks along the chain contour. The other model is the standard Grest-Kremer[85] bead-spring model, amended by the standard cosine potential $U_b(\theta) = \epsilon_b(1 - \cos\theta)$ [Eq. (3)] between neighboring bonds. For large ϵ_b/k_BT, this potential essentially becomes $U_b(\theta) \approx (\epsilon_b/2)\theta^2$, and hence, the model (apart from excluded volume) can be considered as a discretization of the well-known Kratky-Porod model of wormlike chains, Eq. (2), so ϵ_b simply corresponds to the bending rigidity κ_{KP} of that model. Then the persistence length simply is proportional to ϵ_b/k_BT, and this is confirmed by the simulations (see, e.g., Fig. 7(a)). Note that in the presence of excluded volume, a valid definition of the persistence length always is derived from $\langle\cos\theta\rangle$, the average cosine of the angle between neighboring bonds; this is a meaningful measure of local chain stiffness, unlike the asymptotic decay of bond vector correlations for bonds that are far separated along the chain contour (this asymptotic decay is controlled by excluded volume effects, ignored in Eq. (2)).

We have obtained the mean square end-to-end distance of both models in the bulk, applying Monte Carlo methods for the lattice model and molecular dynamics (with a Langevin thermostat) for the off-lattice model. We find that the crossover from the rod-like regime (for contour lengths $L < \ell_p$) to the self-avoiding walk-like regime (described by Eq. (14)) is qualitatively similar in both models, when one studies these linear dimensions as functions of the scaling variable L/ℓ_p (Fig. 3). The amplitude prefactors of the power laws in the asymptotic scaling regime for both models differ slightly, as expected, since only exponents are universal, but not amplitude prefactors. Since in the rod regime the data trivially are model-independent ($\langle R_N^2\rangle = L^2$ for $L \ll \ell_p$), it follows that crossover scaling functions of both models cannot be identical (Fig. 3(b)). In fact, if the asymptotic power law is scaled out, one finds in the crossover scaling functions in the regime $1 < L/\ell_p < 10$ a nontrivial maximum, and there is no universality of these crossover scaling functions. However, when one considers the reduced transverse fluctuation (Fig. 4), one finds in the crossover scaling plot a maximum, whose position is universal, at least within the accuracy of the present estimations, namely, it occurs at $\ln(L/\ell_p) \approx 1$. Providing such a plot from the analysis of experimental AFM pictures of semiflexible polymers adsorbed at planar substrates could be an alternative to the experimental estimation of ℓ_p from the Kratky-Porod formula for the mean square end-to-end distance, which is questionable due to its neglect of excluded volume effects (it describes a crossover to Gaussian coil behavior, which in reality cannot occur). Thus, our comparison of the two studied models is not just an academic exercise but could be a useful guide in practice.

While the disparity of local chain conformations between both models hence has only minor consequences, as far as the bulk properties are concerned, this is no longer true when one considers confinement in strips with $D < \ell_p$. One interesting feature is that in the lattice model, the effective

persistence length $\ell_p(D)$ gets renormalized, while for the continuum model, it remains unchanged (Fig. 7). This discrepancy can be understood from the fact that on the lattice straight sequences of bonds along the y axis get more and more suppressed (Fig. 2(c)), while in the continuum bending of the chain (on scales less than the deflection length λ, cf. Figs. 2(a) and 5 (Multimedia view)) is not affected. A second very interesting discrepancy between both models is that in the continuum model entropic depletion of monomers near the repulsive walls always occurs (Fig. 13), while there is no such depletion for rather stiff lattice chains (Fig. 12). For flexible chains, both on the lattice and in the continuum, near a repulsive boundary depletion does occur, $\rho(y) \propto y^{4/3}$ for $\ell \ll y \ll D$, and the monomer density profile across the strip exhibits a scaling, which is almost universal (again, a simple model-dependent amplitude factor occurs, cf. Eq. (23)). However, for rather stiff chains in the continuum a different power law has been predicted on the basis of the Kratky-Porod model by Semenov,[77] and our data (Fig. 13(b)) seem to be compatible with this prediction. However, while for flexible chains, the chain ends also show an entropic depletion effect, but described by different exponents (Eq. (26)), and this prediction has been verified by both the lattice and the continuum model, no such depletion effect can be detected for semiflexible chains. For $D < \ell_p$, the end monomer profile is almost constant across the strip, both for the lattice and the continuum model (Fig. 14). A third discrepancy is the fact that for the semiflexible bead-spring model, the concept of Odijk[15] of a deflection length (Fig. 2(a)) obviously is applicable for strongly confined chains in the continuum (Fig. 5 (Multimedia view)) but meaningless for the lattice model. We also have discussed the possibility to extract the distribution function $P(\lambda)$ of deflection lengths directly from a statistical analysis of configurations of confined chains in the continuum model. We have shown that after a suitable further coarse-graining of the chain contours, necessary to remove small scale structure, both the average deflection length $\bar{\lambda}$ and the fluctuation $\Delta\lambda \equiv (\overline{\lambda^2} - \bar{\lambda}^2)^{1/2}$ could be obtained. Both $\bar{\lambda}$ and $\Delta\lambda$ are of the same order as predicted (Eq. (1)).

However, for less extreme confinement ($D > \ell_p$) again a remarkable similarity between both models is found: there is a crossover from rods (for $L < \ell_p$) to self-avoiding walks (for chains that are short enough that a single blob fits into the strip) and further to the Daoud-De Gennes string of blobs. For the Monte Carlo results, where a very wide range of L for every choice of ℓ_p is spanned, these three regimes can be easily seen (Fig. 10(b)), but for the MD results, they can also be inferred for appropriate choices of ℓ_p and D. The scaling predictions resulting from the string of blob picture are nicely verified for both models (Fig. 11).

We also note that the snapshot pictures in the regime $\ell_p < D < 3\ell_p$, where well-developed blobs do not yet fit into the strip, clearly reveal hairpin formation, as proposed by Odijk[22] who also has estimated that hairpin formation involves the crossing of a free energy barrier that is proportional to ℓ_p for $D \ll \ell_p$. However, in the regime $D < \ell_p$ where the theory applied, hardly any hairpins could be observed, and hence, our simulations are not suited to test this theory. For the three-dimensional case, a pioneering study of the effects of hairpins on confinement of semiflexible polymers can be found in Ref. 94.

Of course, for addressing experiments, an extension of our study to three dimensions (quasi-one-dimensional confinement in tubes with square, rectangular, or circular cross section) would be very desirable but must be left to future work. We note that in this case several additional complications arise, such as the intermediate Gaussian regime of chain conformational statistics, and knot formation for very long chains.

However, the goal of this study was not to contribute directly to the analysis of experiments but rather to understand how different general assumptions implicit in the choice of particular coarse-grained models do affect the physical properties of the studied macromolecular systems. In particular, we have found in the bulk that the difference in local chain conformations between lattice and continuum models does no longer matter much, when one compares data for the same choice of persistence length (although the dependence of ℓ_p on the energy parameters is very different). Under confinement, the absence of monomer depletion for rather stiff lattice chains shows that discrete bond angles lead to a different physics in comparison to continuous bond angles as possible for the off-lattice model. We have argued, however, that both chains may be physically relevant since different types of mechanisms for chain rigidity occur for cases such as alkane-type polymers or dsDNA.

ACKNOWLEDGMENTS

A.H. and A.B. acknowledge the computational time provided at the STOKES cluster by the Advanced Research Computing Center in University of Central Florida. H.-P.H. is grateful to the Deutsche Forschungsgemeinschaft (DFG) for financial support via Sonderforschungsbereich SFB 625/A3 during the time when she worked at JGU. H.-P.H. and K.B. gratefully acknowledge the computing time granted by the John von Neumann Institute for Computing (NIC) and provided on the supercomputer JUROPA at Jülich Supercomputing Centre (JSC).

[1]W. Reisner, J. N. Pedersen, and R. H. Austin, Rep. Prog. Phys. **75**, 106601 (2012).
[2]J. O. Tegenfeldt, C. Prinz, H. Cao, S. Chou, W. W. Reisner, R. Riehn, Y. M. Wang, E. C. Cox, J. C. Sturm, P. Silberzan, and R. H. Austin, Proc. Natl. Acad. Sci. U. S. A. **101**, 10979 (2004).
[3]W. Reisner, K. J. Morton, R. Riehn, Y. M. Wang, Z. Yu, M. Rosen, J. C. Sturm, S. Y. Chou, E. Frey, and R. H. Austin, Phys. Rev. Lett. **94**, 196101 (2005).
[4]K. Jo, D. M. Dhingra, T. Odijk, J. J. de Pablo, M. D. Graham, R. Runnheim, D. Forrest, and D. C. Schwartz, Proc. Natl. Acad. Sci. U. S. A. **104**, 2673 (2007).
[5]K. Shin, S. Obukhov, J.-T. Chen, J. Huh, Y. Hwang, S. Mak, P. Dobriyal, P. Thiyagarajan, and T. P. Russell, Nat. Mater. **6**, 961 (2007).
[6]D. J. Bonthuis, C. Meyer, D. Stein, and C. Dekker, Phys. Rev. Lett. **101**, 108303 (2008).
[7]P. K. Lin, K.-H. Lin, C.-C. Fu, K.-C. Lee, P.-K. Wei, W.-W. Pai, P.-H. Tsao, Y.-L. Chen, and W. S. Fann, Macromolecules **42**, 1770 (2009).
[8]J. Tang, S. L. Levy, D. W. Trahan, J. J. Jones, H. G. Craighead, and P. S. Doyle, Macromolecules **43**, 7368 (2010).
[9]H. Uemura, M. Ichikawa, and Y. Kimura, Phys. Rev. E **81**, 051801 (2010).
[10]W. Reisner, N. B. Larsen, A. Silahtaroglu, A. Kristensen, N. Tommerup, J. O. Tegenfeldt, and H. Flyvbjerg, Proc. Natl. Acad. Sci. U. S. A. **107**, 13294 (2010).

[11]Y. Kim, K. S. Kim, K. L. Kounovsky, R. Chang, G. Y. Jung, J. J. de Pablo, K. Jo, and D. C. Schwartz, Lab Chip **11**, 1721 (2011).
[12]T. Su, S. K. Das, M. Xiao, and P. K. Purohit, PLoS One **6**, e16890 (2011).
[13]K. D. Dorfman, D. Gupta, A. Jain, A. Muralidhar, and D. R. Tree, Eur. Phys. J.: Spec. Top. **223**, 3179 (2014).
[14]W. F. Reinhart, J. G. Reifenberger, D. Gupta, A. Muralidhar, J. Sheats, H. Cao, and K. D. Dorfman, J. Chem. Phys. **142**, 064902 (2015).
[15]T. Odijk, Macromolecules **16**, 1340 (1983).
[16]T. Odijk, Macromolecules **17**, 502 (1984).
[17]T. Odijk, Macromolecules **19**, 2313 (1986).
[18]T. W. Burkhardt, J. Phys. A **30**, L167 (1997).
[19]G. Morrison and D. Thirumalai, J. Chem. Phys. **122**, 194907 (2005).
[20]J. Z. Y. Chen and D. E. Sullivan, Macromolecules **39**, 7769 (2006).
[21]S. Jun, D. Thirumalai, and B.-Y. Ha, Phys. Rev. Lett. **101**, 138101 (2008).
[22]T. Odijk, Phys. Rev. E **77**, 060901(R) (2008).
[23]Y. Jung, S. Yun, and H.-Y. Ha, Phys. Rev. E **79**, 061912 (2009).
[24]F. Thüroff, R. Wagner, and E. Frey, EPL **91**, 38004 (2010).
[25]F. Thüroff, B. Obermayer, and E. Frey, Phys. Rev. E **83**, 021802 (2011).
[26]Y.-L. Chen, M. D. Graham, J. J. de Pablo, G. C. Randall, M. Gupta, and P. S. Doyle, Phys. Rev. E **70**, 060901(R) (2004).
[27]P. Cifra, J. Chem. Phys. **131**, 224903 (2009).
[28]P. Cifra, Z. Benková, and T. Bleha, J. Phys. Chem. B **113**, 1843 (2009).
[29]Y. Wang, D. R. Tree, and K. D. Dorfman, Macromolecules **44**, 6594 (2011).
[30]P. Cifra, J. Chem. Phys. **136**, 024902 (2012).
[31]D. R. Tree, Y. Wang, and K. D. Dorfman, Phys. Rev. Lett. **110**, 208103 (2013).
[32]J. Z. Y. Chen, Macromolecules **46**, 9837 (2013).
[33]L. Dai and P. S. Doyle, Macromolecules **46**, 6336 (2013).
[34]H.-P. Hsu and K. Binder, Soft Matter **9**, 10512 (2013).
[35]H.-P. Hsu and K. Binder, Macromolecules **46**, 8017 (2013).
[36]A. Huang and A. Bhattacharya, EPL **106**, 18004 (2014).
[37]A. Muralidhar, D. R. Tree, Y. Wang, and K. D. Dorfman, J. Chem. Phys. **140**, 0849905 (2014).
[38]L. Dai, J. van der Maarel, and P. S. Doyle, Macromolecules **47**, 2445 (2014).
[39]Z. Benková, P. Námer, and P. Cifra, Soft Matter **11**, 2279 (2015).
[40]M. Daoud and P. G. De Gennes, J. Phys. (Paris) **38**, 85 (1977).
[41]P. de Gennes, *Scaling Concepts in Polymer Physics* (Cornell University Press, Ithaca, NY, 1979).
[42]K. Kremer and K. Binder, J. Chem. Phys. **81**, 6381 (1984).
[43]A. Milchev, W. Paul, and K. Binder, Macromol. Theory Simul. **3**, 305 (1994).
[44]P. Sotta, A. Lesne, and J. M. Victor, J. Chem. Phys. **112**, 1565 (2000).
[45]Y. Yang, T. W. Burkhardt, and G. Gompper, Phys. Rev. E **76**, 011804 (2007).
[46]H.-P. Hsu and P. Grassberger, Eur. Phys. J. B **36**, 209 (2003).
[47]R. M. Jendrejack, E. T. Dimalantha, D. C. Schwartz, M. D. Graham, and J. J. de Pablo, Phys. Rev. Lett. **91**, 038102 (2003).
[48]R. M. Jendrejack, D. C. Schwartz, M. D. Graham, and J. J. de Pablo, J. Chem. Phys. **119**, 1165 (2003).
[49]H.-P. Hsu, K. Binder, L. I. Klushin, and A. M. Skvortsov, Phys. Rev. E **76**, 021108 (2007).
[50]H.-P. Hsu, K. Binder, L. I. Klushin, and A. M. Skvortsov, Phys. Rev. E **78**, 041803 (2008).
[51]W. Humphrey, A. Dalke, and K. Schulten, J. Mol. Graphics **14**, 33 (1996).
[52]L. I. Klushin, A. M. Skvortsov, H.-P. Hsu, and K. Binder, Macromolecules **41**, 5890 (2008).
[53]A. Milchev, L. Klushin, A. Skvortsov, and K. Binder, Macromolelcues **43**, 6877 (2010).
[54]D. W. Schaefer, J. F. Joanny, and P. Pincus, Macromolecules **13**, 1280 (1980).
[55]H. Nakanishi, J. Phys. (Paris) **48**, 979 (1987).
[56]J. Moon and H. Nakanishi, Phys. Rev. A **44**, 6427 (2012).
[57]H.-P. Hsu and K. Binder, J. Chem. Phys. **136**, 024901 (2012).
[58]A. Yu Grosberg and A. R. Khokhlov, *Statistical Mechanics of Chain Molecules* (AIP Press, New York, 1994).
[59]J. C. Le Guillou and J. Zinn-Justin, Phys. Rev. B **21**, 3976 (1980).
[60]H.-P. Hsu, W. Paul, and K. Binder, EPL **95**, 68004 (2011).
[61]T. Odijk, J. Chem. Phys. **125**, 204904 (2006).
[62]O. Kratky and G. Porod, Recl. Trav. Chim. Pays-Bas **68**, 1106 (1949).
[63]O. Kratky and G. Porod, J. Colloid Sci. **4**, 35 (1949).
[64]C. Bustamante, J. F. Markov, E. D. Siggia, and S. Smith, Science **265**, 1599 (1994).
[65]D. A. D. Parry and E. N. Baker, Rep. Prog. Phys. **47**, 1133 (1984).
[66]J. T. Titantah, C. Pierleoni, and J.-P. Ryckaert, J. Chem. Phys. **117**, 9028 (2002).
[67]M. Rawiso, R. Duplessix, and C. Picot, Macromolecules **20**, 630 (1987).
[68]J. S. Pedersen and P. Schurtenberger, Europhys. Lett. **45**, 666 (1999).
[69]T. Norisuye and H. Fujita, Polym. J. **14**, 143 (1982).
[70]G. Maurstad, S. Danielsen, and B. T. Stokke, J. Phys. Chem. B **107**, 8172 (2003).
[71]A. R. Khokhlov and A. R. Semenov, Macromolecules **17**, 2678 (1984).
[72]P. J. Flory, *Statistical Mechanics of Chain Molecules* (Interscience, New York, 1969).
[73]C. Hyeon and D. Thirumalai, Nat. Commun. **2**, 487 (2011).
[74]F. Latinwo and C. M. Schroeder, Soft Matter **7**, 7907 (2011).
[75]R. G. Winkler, P. Reineker, and L. Harnau, J. Chem. Phys. **101**, 8119 (1994).
[76]T. Vogel, T. Neuhaus, M. Bachmann, and W. Janke, Phys. Rev. E **80**, 011802 (2009).
[77]A. N. Semenov, Eur. Phys. J. E **9**, 353 (2002).
[78]H.-P. Hsu, W. Paul, and K. Binder, Macromolecules **43**, 3094 (2010).
[79]H.-P. Hsu, W. Paul, and K. Binder, EPL **92**, 28003 (2010).
[80]A. Huang, A. Bhattacharya, and K. Binder, J. Chem. Phys. **140**, 214902 (2014); EPL **105**, 18002 (2014).
[81]L. F. Liu, L. Perkocha, R. Calendar, and J. C. Wang, Proc. Natl. Acad. Sci. U. S. A. **78**, 5498 (1981).
[82]V. V. Rybenkov, N. R. Cozzarelli, and A. V. Vologodskii, Proc. Natl. Acad. Sci. U. S. A. **90**, 5307 (1993).
[83]P. Grassberger, Phys. Rev. E **56**, 3682 (1997).
[84]H.-P. Hsu and P. Grassberger, J. Stat. Phys. **144**, 597 (2011).
[85]G. S. Grest and K. Kremer, Phys. Rev. A **33**, 3628 (1986).
[86]W. F. van Gunsteren and H. J. C. Berendsen, Mol. Phys. **45**, 637 (1982).
[87]D. Reith, H. Meyer, and F. Müller-Plathe, Macromolecules **34**, 2335 (2001).
[88]H. Yamakawa and M. Fujii, J. Chem. Phys. **59**, 6641 (1973).
[89]A. Caspi, M. Elbaum, R. Granek, A. Lachish, and D. Zbaida, Phys. Rev. Lett. **80**, 1106 (1998).
[90]J. Moukhtar, E. Fontaine, C. Faivre-Moskalenko, and A. Arneodo, Phys. Rev. Lett. **98**, 178101 (2007).
[91]J. Moukhtar, C. Faivre-Moskalenko, P. Milani, B. Audit, C. Vaillant, E. Fontaine, F. Mongelard, G. Lavorel, P. St-Jean, P. Bouvet, F. Argoul, and A. Arneodo, J. Phys. Chem. B **114**, 5125 (2010).
[92]E. Eisenriegler, K. Kremer, and K. Binder, J. Chem. Phys. **77**, 6296 (1982).
[93]E. Eisenriegler, *Polymers Near Surfaces* (World Scientific, Singapore, 1993).
[94]A. Muralidhar, D. R. Tree, and K. D. Dorfman, Macromolecules **47**, 8446 (2014).